INTERNATIONAL JOURNAL OF AUTOMOTIVE AND MECHANICAL ENGINEERING
ISSN: 2229-8649 e-ISSN: 2180-1606
VOL. 21, ISSUE 2, 2024, 11415 – 11425
DOI: https://doi.org/10.15282/ijame.21.2.2024.18.0881

RESEARCH ARTICLE

Investigation of Brake Pad Wear Impact on Autonomous Emergency Braking Pedestrian Performance on Wet Road Conditions

Z. Abdullah[1]*, P.M. Heerwan[1,2]*, M.A. Zakaria[2,3] and M.I. Ishak[1,2]

[1]Faculty of Mechanical and Automotive Engineering Technology, Universiti Malaysia Pahang Al-Sultan Abdullah, 26600 Pekan, Pahang, Malaysia
[2]Automotive Engineering Center, Universiti Malaysia Pahang Al-Sultan Abdullah, 26600 Pekan, Pahang, Malaysia
[3]Faculty of Manufacturing and Mechatronics Engineering and Technology, Universiti Malaysia Pahang Al-Sultan Abdullah, 26600 Pekan, Pahang, Malaysia

ABSTRACT - This study presents an investigation of autonomous emergency braking pedestrian (AEB-P) system performance during harsh braking on wet road pavement. The system was designed to consider a pedestrian walking in front of the host vehicle. The performance of the AEB-P system would degrade immediately as the pads on the brakes become worn, and the vehicle continues to brake on a wet road surface. The vehicle conditional artificial potential field (VC-APF) is an innovative approach for motion planning in the AEB-P introduced in this work. The simulation was performed to explore the impact of brake pad degradation on VC-APF effectiveness on wet road pavement. The first evaluation involved a test to evaluate the effectiveness of the risk assessment in the AEB-P system when encountering a moving obstacle (pedestrian). The second test evaluated VC-APF performance, for instance, the vehicle's safety distance when the vehicle performed hard braking at 0.4, 0.35, and 0.24 brake pad friction coefficients. The third evaluation focused on the vehicle's speed behavior during deceleration at various brake pad friction coefficients. The simulation results showed that while braking at 0.4 and 0.35 brake pad friction coefficients, the vehicle maintained a minimum safety distance of 1.5 m and 0.69 m from a pedestrian on wet road pavement, respectively. However, the brake pad friction coefficient of 0.24 failed to prevent the vehicle from crashing. The findings indicate that an exhausted brake pad reduces the vehicle's safety.

ARTICLE HISTORY
Received : 21st Dec. 2023
Revised : 26th Apr. 2024
Accepted : 17th May 2024
Published : 20th June 2024

KEYWORDS
Brake pad wear,
Autonomous emergency braking pedestrian,
Vehicle conditional artificial potential field,
Vehicle safety,
Brake performance.

1.0 INTRODUCTION

Pedestrian-vehicle accidents represent by far the most serious kind of disaster due to their high casualty percentage. There were about 316,000 occurrences of road disasters in the ASEAN region, resulting in an accident rate of 17.0 per 100,000 people. This rate was just under the global rate of 17.4% [1]. Vulnerable road users (VRUs), comprised of walkers, motorcyclists, and cyclists, accounted for half of the region's road traffic deaths, with pedestrians accounting for 13% [1]. According to the preceding reference, pedestrians are the common victims of traffic crashes. Pedestrians in metropolitan areas encounter a variety of pedestrian and vehicle-related activities, which makes them the most vulnerable category [1]. The data show that straight roads account for the most pedestrian fatalities, followed by junction-type roads in terms of incident circumstances.

In Malaysia, frontal crashes are the typical type of hazard, as per the data from the Malaysian Institute of Road Safety Research [1]. The type of obstacle (vehicle, pedestrian, or edge of the road), the impact speed, and its configuration determine the collision scenario [2]. When two vehicles collide, factors such as crash speed, collision direction, vehicle mismatch, driver characteristics (e.g., gender, age, car size), and vehicle safety devices all play a major role in determining the severity of the collision. Additionally, the data investigation on pedestrian crashes revealed that pedestrians were struck by light commercial vehicles [3]. Road users may struggle to balance mobility and safety while driving. The accident rate tends to increase as the average traffic speed increases, specifically for VRUs. An adult pedestrian has a lower than 20% probability of colliding when the vehicle is traveling at an approximate speed of 50 km/h. However, when struck by a vehicle at 80 km/h, the chances of survival are only about 40% [1].

Experts are focusing on advanced driver assistance system (ADAS) using useful concepts like automatic emergency braking (AEB) to reduce the number of pedestrian injuries. Automatic emergency braking systems have been shown to work efficiently at low speeds, leading to a 35%–41% reduction in overall collisions [4]. On the other hand, collisions and injury cases have decreased by 54%–57% [4]. Only 35%–42% of collisions are avoided at a velocity of 60–70 km/h, while only 35%–42% of crashes are evaded at speeds lower than or equivalent to 50 km/h. At a velocity of 80 km/h or more, the host vehicle only eliminates 12%–25% of the risk [5]. In accordance with the police-reported accident study, a car with AEB assistance was involved in 38% fewer instances than vehicles with no AEB assistance [5]. The threat assessment, path planning, and path tracking modules are critical elements of the architecture of an AEB system. Each approach contains features that enable the AEB system to operate properly.

***CORRESPONDING AUTHOR | Z. Abdullah, P.M. Heerwan** | ✉ abdullahzulkifli27@gmail.com, mheerwan@umpsa.edu.my

Accidental accidents, such as a car colliding with an obstacle, can be prevented by using threat assessment (TA) as a safety precaution, allowing for a collision-free route. The TA module needs to access information about the lead vehicle, such as speed, position, and travel direction, to recalculate the risk on the road [6]. The TA's warning and overriding mechanisms alert drivers in two distinct ways [7]. Time-to-collision (TTC) is a popular TA method [7]. The TTC is calculated utilizing the speed and distance variables between a vehicle and an obstacle. After the TA has discovered the threat or risk, an overriding framework, known as a path-planning system, will reconsider the current route in order to prevent the obstacle [8]. Path planning must provide a set of predefined pathway forecasts to allow the vehicle to avoid obstacles or change lanes. As dynamic barriers require only a small amount of processing power, the sensor's online path planning is routinely utilized [9], [10], [11]. A kinematic path planner was selected as a small change in direction is sufficient to address the collision-avoidance aim in a simple situation [12]. A fundamental vehicle kinematic model and an uncomplicated algorithm were used to generate the future replanned path [12]. This enables fast trajectory replanning.

The artificial potential field (APF) technique was adopted by the authors in [8], whereby the robot is pushed by a combination of repulsive and attractive forces in the environment. This strategy is easy to understand and apply. The attractive force drew the robot to its destination, while the repellent force pushed the robot away from a barrier [13], [14]. Fortunately, significant work has been achieved recently to improve the standard method by incorporating dynamic and environmental constraints into the algorithm [15]. As an outcome of this method, the vehicle was no longer caught in local minima. Ultimately, by modifying the formulation of the potential field, an optimal replanned route was determined [16]. The path-tracking strategy will follow the trajectory from the path-planning method once the revised collision-avoiding path has been generated. A single-input and single-output system is a simple and straightforward tracking system that provides a fast response output. The typical approach is a well-known technique utilized by a scientist to change the route planner's real path into the desired path. One of the classic techniques for controlling the trajectory involves the proportional integral derivative (PID) control [17].

The coefficient of friction caused by the tires of the cars and the pavement defines the maximum potential velocity and, thus, the shortest feasible stopping distances [18]. According to [19], the norm for the wet friction coefficient that was used was approximately 0.6. Although an autonomous emergency braking pedestrian (AEB-P) system can prevent an accident, its effectiveness will suffer if braking is performed on a slippery road pavement. Brake fading is another problem that can affect AEB-P effectiveness. It can be caused by several factors, including exhaust brake pads. The degradation of the pads' material's binder stage, such as phenolic resin, is the essential root of this event. On a mesoscopic scale, the resin has deteriorated to its limit of discharging [20]. Due to these operations, the patches of contact have significantly grown, leading to a decrease in the frictional coefficient of the brake pad's surface [20]. This occurs because the brake system overheats, leading to a loss of braking power. During the braking behavior, the outermost layer of the brake pad must maintain a steady high temperature and an equal coefficient of friction. To prevent brake fading caused by thermal strain during single or multiple brakes in situations of rapid speed or massive load conditions, the drainage capabilities and thermal storage of the brake system's components must be addressed [21]. The braking pattern might also cause brake fading [21]. As stated by [22], the typical values of the friction coefficient are 0.35–0.38, 0.39–0.43, and 0.16–0.24, corresponding to brake pad fatigue temperatures at small, intermediate, and extreme heat levels of 100–150 °C, 200–250 °C, and 300–350 °C, respectively. The pad's wear test is equal at low, intermediate, and high temperatures when the vehicle stops at slower speeds, with harsher braking, and with substantial emergency braking [22].

According to the literature review, two elements may impact AEB-P effectiveness: the road pavement and the state of the brake pads. The influence of road pavement and brake pad wear was investigated in this research utilizing the vehicle conditional artificial potential field (VC-APF) and a kinematic motion planner on the AEB-P system. The simulation was performed on a wet pavement surface, and the degree of brake pad wear was calculated by adjusting the coefficient of friction of the brake pads between 0.4, 0.35, and 0.24. The AEB-P performance was evaluated based on the vehicle's dynamic and actuator responses. There are four sections in this paper. The first part includes an introduction and a summary of relevant earlier research. The second part includes the methodology of this study, such as the vehicle model and AEB-P system development in MATLAB Simulink. The third part discusses the AEB-P system performance in terms of TTC with an obstacle, minimum safety distance after harsh braking, as well as the velocity of the vehicle. The last part of this paper presents the conclusion of this research.

2.0 METHODOLOGY

2.1 Analysis Vehicle Model

Figure 1 depicts the Proton Persona, the analytical car model utilized for simulation. Table 1 shows the key characteristics of this vehicle. The forces exerted on the vehicle are used to generate the vehicle equations of motion in the simulations. Figure 2 depicts the braking forces at each tire.

Figure 1. Proton Persona vehicle model

Table 1. The specification of the analysis vehicle model

Details	Symbol	Value	SI unit
Vehicle mass	m	1,330	kg
Length toward the frontal part from the center of gravity	l_f	1.107	m
Length toward the rear part from the center of gravity	l_r	1.643	m
Centre gravity's height	h	0.479	m
Tire's effective radius	r_{eff}	0.393	m

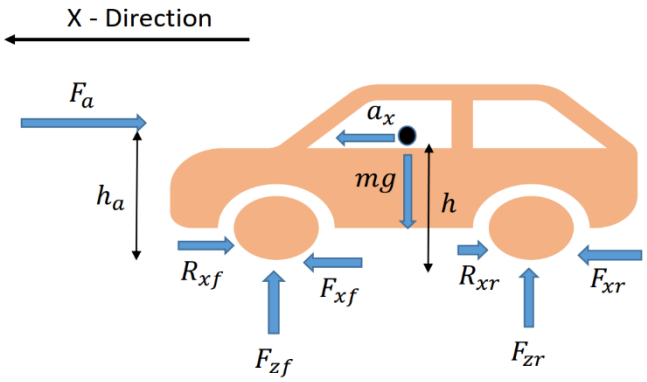

Figure 2. Force acting on the longitudinal axis at each tire

As this study is solely concerned with braking along the longitudinal axis, the dynamics equation of motion for this vehicle along the longitudinal axis is given by Eq.1:

$$m_{ax} = F_{xfl} + F_{xfr} + F_{xrl} + F_{xrr} \tag{1}$$

where m represents the vehicle mass, a_x represents longitudinal deceleration, and F_{xfr}, F_{xfl}, F_{xrr}, and F_{xrl} represent the longitudinal forces at each tire. As shown in Eq. 2, the longitudinal force at every tire was calculated utilizing a nonlinear tire approach, which is the Dugoff tire model [23]:

$$F_x = C_\sigma \frac{\sigma_x}{1+\sigma_x} f(\lambda) \tag{2}$$

where C_σ stands for the longitudinal tire stiffness, while σ_x denotes the slip ratio in the longitudinal direction. The function $f(\lambda)$ and variable, λ is one of the parameters included in the Dugoff tire model and shown in Eq. 3 and Eq. 4, respectively.

$$f(\lambda) = \begin{cases} (2-\lambda)\lambda, & \lambda < 1 \\ 1 \quad , & \lambda \geq 1 \end{cases} \tag{3}$$

$$\lambda = \frac{\mu F_z (1+\sigma_x)}{2[(C_\sigma \sigma_x)^2 + (C_a \tan(\beta))^2]^{1/2}} \tag{4}$$

According to Eq. 4, μ denotes the tire-road coefficient friction, while F_z is the dynamic load at each tire. β stands for the tire side slip angle and can be neglected during braking along the longitudinal axis in the simulation. The equation of μ relies on the road surface, as illustrated in Eq. 5. The road friction coefficient can be denoted as k and is set to 0.6 in the simulation for the wet surface [24].

$$\mu = -1.15k \{e^{-35\sigma_x} - e^{-0.35\sigma_x}\} \tag{5}$$

Eqs. 6, 7, and 8 express the wheel dynamic model. T_f, T_{br}, and I_{tire} stand for the tire's traction torque, braking torque, and inertia, respectively. The braking torque will be subtracted from the traction torque and divided by the tire's inertia to produce the tire's angular acceleration, as expressed in Eq. 6.

$$\frac{T_f - T_{br}}{I_{tire}} = \frac{d\omega}{dt} \tag{6}$$

The wheel's angular velocity can be determined by integrating the wheel's angular acceleration with respect to time, as shown in Eq.7. Next, the wheel's velocity can be determined by multiplying the wheel's angular velocity with the tire's radius, as expressed in Eq. 8.

$$\int \frac{d\omega}{dt} = \omega_v \tag{7}$$

$$V_t = r_{tire}\omega_v \tag{8}$$

The slip ratio can be estimated by studying the vehicle and tire speed. The longitudinal slip ratio while decelerating is given by Eq. 9:

$$\sigma_x = \frac{V_t - V_x}{V_x} \tag{9}$$

2.2 Architecture of AEB-P

The AEB control approach usually relies on the TTC between the host vehicle and the following car or obstacle. The innovative strategy in this study is to take the risk of pedestrians crossing the sidewalk into account in the AEB equation. Figure 3 depicts the framework of the suggested AEB-P system technique. The TTC is the risk evaluation of the surroundings in a dangerous or safe situation, as shown in Figure 3. Assume the car is getting close to the AEB activation threshold. Under that situation, the APF and kinematic path planners will react appropriately and provide the PI controller with the best possible deceleration. The following topic goes into detail about each component of the AEB-P system.

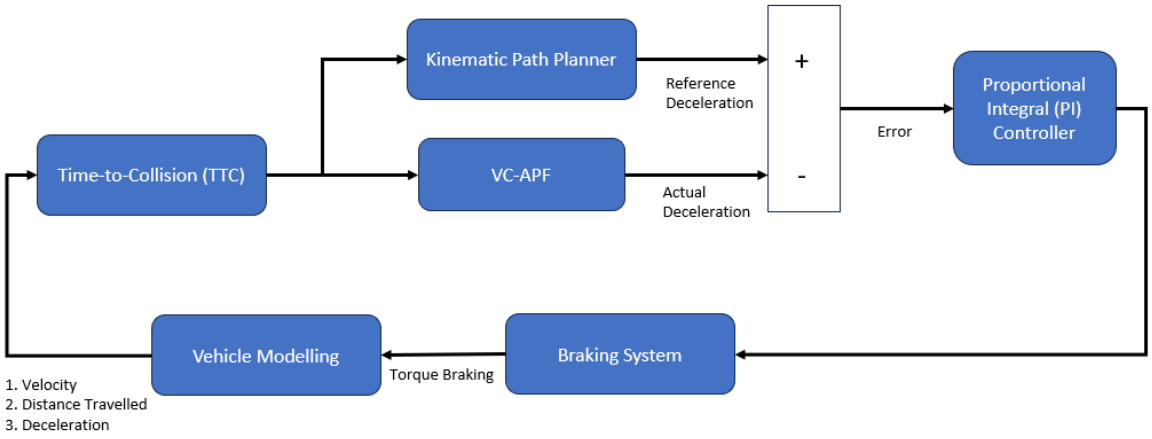

Figure 3. AEB-P architecture system

2.3 Time-to-Collision

TTCv, TTCe, and TTCp constitute the three additional TTCs in this AEB-P architecture. TTCv represents when a pedestrian walking reaches the roadway boundary, TTCe indicates when a pedestrian safely crosses the path of the road, and TTCp reflects the period that passes from the TTCv to the TTCe. Figure 4 depicts driving possibilities with a pedestrian crossing a street. According to Figure 4, an accident will occur when TTCv ≤ TTC ≤ TTCe, and a collision will occur when TTCp ≤ TTCe [25].

The vehicle's starting distance of separation to the pedestrian walkway location was set to 120 m (about 393.7 ft) in the simulation settings. Both the car and the pedestrian are moving at a steady pace of 60 and 4.32 km/h, respectively [26]. The x1 displacement represents a margin of safety as the pedestrian approaches the traffic path, and the x2 displacement represents a safe buffer as the pedestrian exits the roadway lane.

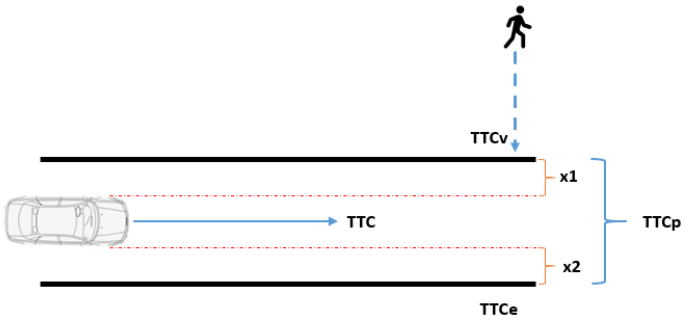

Figure 4. Driving scenario during the presence of a pedestrian

The kinematic approach is used to compute the TTC. When the vehicle in question encounters an obstacle, the TTC is estimated by calculating the formula of the kinematic method, as shown below [27].

$$|p| = \begin{cases} -vt & , \quad \alpha = 0 \\ -vt + \frac{1}{2}\alpha t^2 , & \alpha \neq 0 \end{cases} \tag{10}$$

The speed and deceleration of the host vehicle are given by v and α, respectively. The sign t represents the time it would take for the host vehicle to travel a given distance, whereas p represents the amount of time traveled. Rearranging Eq. 10 yields the collision time, as shown in Eq. 11.

$$|TTC| = \begin{cases} p/v , & v \geq 0 , \alpha = 0 \\ \dfrac{-v \pm \sqrt{v^2 - 2p\alpha}}{\alpha}, & v \geq 0 , \alpha < 0 \end{cases} \tag{11}$$

2.4 Kinematic Path Planner

When an obstacle occurs in front of the host vehicle, the kinematic path planner method can be calculated from the kinematic formula. Figure 5 depicts the kinematic route planner's threshold triggering, which includes the TTC and the maximum safe braking distance, ρ_{or}.

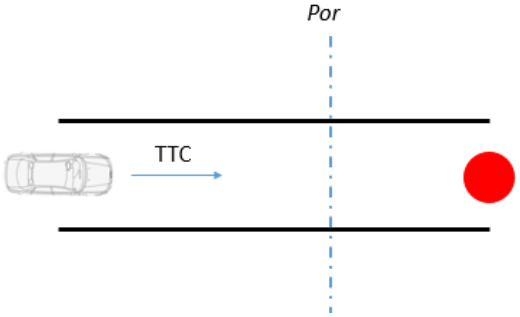

Figure 5. Threshold activation for a kinematic path planner

The kinematic route planning threshold formula, ρ_{or} i given in Eq. 12, where d_0, v_c, and α_{max} stand for the critical safe distance (2 m), the host vehicle speed, and the maximum vehicle deceleration, respectively.

$$\rho_{or} = d_a + (v_c \times TTC) \frac{{v_c}^2}{2\alpha_{max}} \tag{12}$$

The kinematic route planning threshold, also known as the maximum acceptable distance when driving, fluctuates based on the vehicle's speed, peak deceleration, and distance to an object. This route planning threshold violation occurs when the vehicle's spacing headway, ρ_r exceeds the maximum safe distance, ρ_{or}, as shown in Eq. 13. When $\rho_r \leq \rho_{or}$, the maximum deceleration is set to 8 m/s^2, and it yields to the braking system to produce torque braking at each tire [28].

$$\alpha_k = \begin{cases} 8, & \rho_r \leq \rho_{or} \\ 0, & \rho_r > \rho_{or} \end{cases} \tag{13}$$

2.5 Unified Risk Assessment

The TA and the VC-APF path planner are combined in the unified risk evaluation. Whenever the host vehicle is in a sophisticated collision avoidance scenario, this combination is necessary. The pedestrian model details, the obstacle profile, and the vehicle model information must all be accurate when incorporated into the algorithm. A unified risk assessment is depicted in Figure 6.

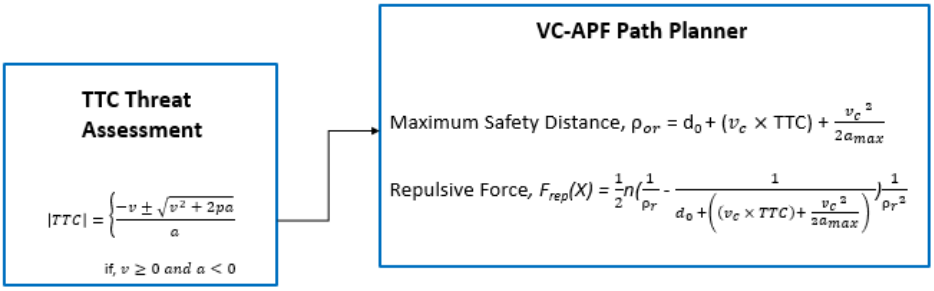

Figure 6. Unified risk assessment

The TA provides the estimated time for a vehicle-pedestrian accident to the VC-APF path planner. The VC-APF is a comprehensive risk assessment derived from the classic APF that is developed whenever the AEB-P system identifies an obstacle in the longitudinal lane. The greater the repulsion force at the obstacles, the shorter the distance that lies between the vehicle and the pedestrian. Figure 7 depicts how the magnitude of repulsion force varies with the threat intensity phase.

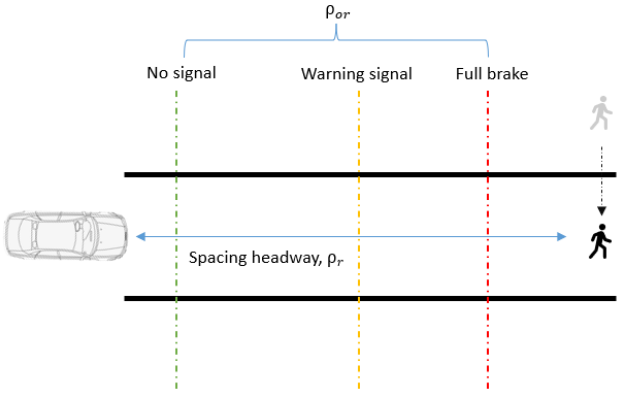

Figure 7. AEB-P system activation phase

The traditional APF is modified by incorporating the vehicle's travel phase, specifically no signal, warning signal, and complete brake [27]. The greater the repellent effect generated at the core of the obstacle, the less space there is separating the vehicle from the obstacle [15]. Eqs. 14, 15, and 16 represent the AEB-P system's complete braking, warning signal, and free states, as depicted in Figure 7, respectively.

$$F_{rep}X = \frac{n}{2}\left(\frac{1}{\rho_r} - \frac{1}{\rho_{or}}\right)\frac{1}{\rho_r^2} \text{ if, } \rho_r \leq \rho_{or} \tag{14}$$

$$F_{rep}X = 0 \text{ (warning signal) if, } \rho_{or} \leq \rho_r \leq \rho_{or} + 1.5 \tag{15}$$

$$F_{rep}X = 0 \text{ (no signal) if, } \rho_r \geq \rho_{or} + 1.5 \tag{16}$$

Eq. 17 expresses the VC-APF path planner that generates a deceleration.

$$\alpha_{VC-APF} = \frac{F_{rep}X}{m} \tag{17}$$

2.6 Braking System

The optimum braking force distribution produced by VC-APF path planning, F_{opt} is expressed in Eq. 18, where α_{pi} and m stand for the desired trajectory deceleration that has been fetched from the PI controller and the mass of the vehicle, respectively.

$$F_{opt} = m \times \alpha_{pi} \tag{18}$$

To keep the back of the tire from locking and to provide enough stopping power to the front tire, each tire needs to have a sufficient amount of braking force. For an AEB-P system to experience load transfer phenomena during activation, a practical braking force must be applied at each tire. The vehicle's free body diagram, which is depicted in Figure 8, comprises the length between the front tire's center of gravity, L_f, and the rear tire's center of gravity, L_r. The optimum braking force produced by VC-APF path planning was multiplied by the percentage of the length between the front tire and the center of gravity over the length between the front and rear tires to obtain the braking force at the rear tire. The braking force at the front tire was calculated as the output between the optimum braking force produced by VC-APF path planning with the percentage of the length between the rear tire and the center of gravity over the length between the front and rear tires.

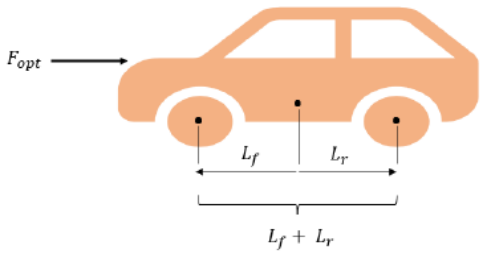

Figure 8. Force distribution at each tire

Braking force at the rear tire, F_{br}:

$$F_{br} = F_{opt} \times \left(\frac{L_f}{L_f + L_r} \times 100 \right) \tag{19}$$

Braking force at the front tire, F_{bf}:

$$F_{bf} = F_{opt} \times \left(\frac{L_r}{L_f + L_r} \times 100 \right) \tag{20}$$

This disc braking system serves as an actuator for the AEB-P system. The performance of the braking system is directly impacted by the coefficient of friction at the brake disc pad. Figure 9 depicts the contact patch between the disc rotor and the brake pad.

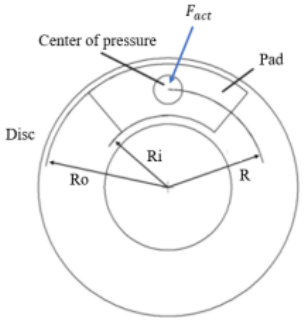

Figure 9. Contact patch between the brake pad and the disc rotor

The braking torque, T_b is created by multiplying the actuating force operating on the center of pressure, F_{act} and the effective radius, R. The force that gripped the disc brake is represented by F_{clamp}. To produce retarding torque on disc brakes, the actuating forces press the piston against the rotor. $F_{friction}$ is the frictional force that develops at the disc brake due to the application of an actuation force.

$$F_{clamp} = 2F_{act} \tag{21}$$

$$F_{friction} = \mu F_{clamp} \tag{22}$$

$$T_{br} = F_{friction}\mathrm{R} \tag{23}$$

The braking torque on disc brakes can be written as in Eq. 23. In the simulation, F_{act} is the optimum braking force, F_{opt}, that has been obtained from the unified risk assessment and PI controller tuning.

$$T_{br} = 2\mu_{disc}F_{act}\mathrm{R} \tag{24}$$

To investigate the effect of the brake pad, the value of the coefficient of friction of the brake pad, which is μ_{disc}, was varied in this simulation. The simulation was conducted at μ_{disc} values equal to 0.4, 0.35, and 0.24. Eqs. 24 and 25 indicate the ABS mechanism on a wet road surface condition, where σ_{down} is 0.145 and σ_{up} is 0.05.

$$T_{br} = 0 \quad when, \sigma_x > \sigma_{down} \tag{24}$$

$$T_{br} = 2\mu_{disc}F_{act}R \quad when, \sigma_x < \sigma_{up} \tag{25}$$

3.0 RESULTS AND DISCUSSION

3.1 Risk Assessment

Figures 10 (a), (b), and (c) depict the TTC for different values of the brake pad's friction coefficients when braking on a wet roadway surface, which are 0.4, 0.35, and 0.24, respectively. The blue and red lines denote the TTC for the host

vehicle and the time first calculated from the pedestrian passing through the collision domain, respectively, whereas the purple and yellow lines represent the times when the pedestrian exited and reached the collision zone, respectively. At 4.285 s, the pedestrian began to approach the accident area. The AEB-P system was activated when the vehicle's time-to-collision (TTC Car) was within the required time limit necessary for the pedestrian to arrive (TTCv) and exit (TTCe) the collision area. The car entered the accident area at 3.1656 s. However, due to the car's speed, the graph for the TTC of the vehicle began to oscillate severely around 4.1248 s until the vehicle completely stopped or impacted the pedestrian. As the magnitude corresponding to the brake pad friction coefficient increased, so did the frequency of the oscillation pattern.

The friction coefficient of the brake pads correlates to the amount of torque braking. Whenever torque braking is applied substantially to the vehicle, the vehicle's velocity drops immediately when the system activation distance for the entire braking phase is recalculated to reduce the full braking stage distance value. This ensures that the spacing headway does not exceed the complete braking distance. When the vehicle velocity does not decelerate sufficiently, the complete braking phase distance is recalculated to ensure that the spacing headway distance is within a certain range of the full brake distance. As indicated in Eqs. 14 and 15, this occurrence will happen regularly until the vehicle completely stops or collides with the pedestrian. The oscillation behavior of the vehicle's TTC would be reduced when the value of the disc's brake pad friction coefficient decreased.

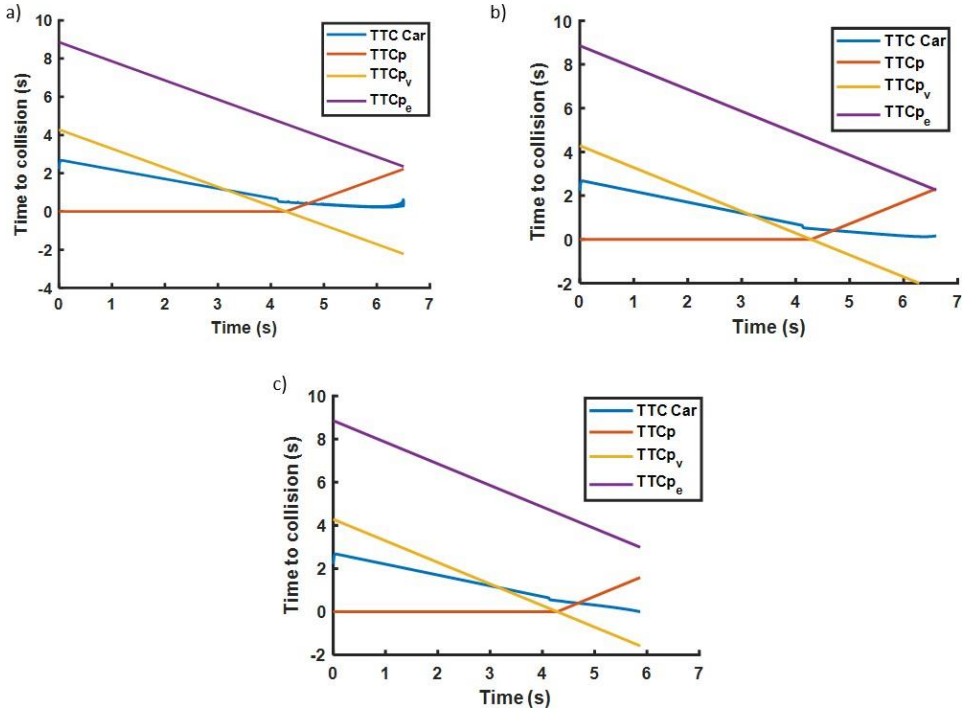

Figure 10. Time to collision of the vehicle and pedestrian against time at (a) μ_{disc} = 0.4, (b) μ_{disc} = 0.35, and (c) μ_{disc} = 0.24 on a wet road surface

3.2 AEB-P System Activation

Figures 11 (a), (b), and (c) depict the AEB-P system engagement when the coefficient of friction for the brake disc pad values are 0.4, 0.35, and 0.24, respectively. The blue line denotes the vehicle's spacing headway, while the red and yellow lines denote the warning signal and full braking phase, respectively. The shape of the warning signal and full braking phase remained consistent throughout the time in an interval of 0–3.166 s and suddenly increased, indicating a distance toward the pedestrian of 35.64 m and 10.67 m, respectively. Eqs. 10 and 14 states that the value of TTC for the vehicle and pedestrian impacted the degree of system activation distance when the pedestrian reached the collision area at 3.1656 s. The host vehicle crossed the warning signal phase range at 37.29 m and the full brake phase distance at 21.313 m from the obstacle.

When the disc friction coefficient was 0.4, the yellow line began to vibrate lightly at 4.3 s and 16.81 m from the obstacle. This is because the spacing headway enters abruptly, exits the region of maximum safety distance from the accident location, and has a direct impact on the activation of the AEB-P system. As the value of the brake pad coefficient of friction decreased, so did this phenomenon. As the reduction in the value of the brake pad friction coefficient will immediately decrease the value of the torque braking, the vehicle will not experience a significant slowdown.

According to the results, the host vehicle stopped at 1.5 m and 0.69 m from the pedestrian for μ_{disc} values of 0.4 and 0.35, respectively. However, when the μ_{disc} was 0.24, the vehicle collided with the pedestrian.

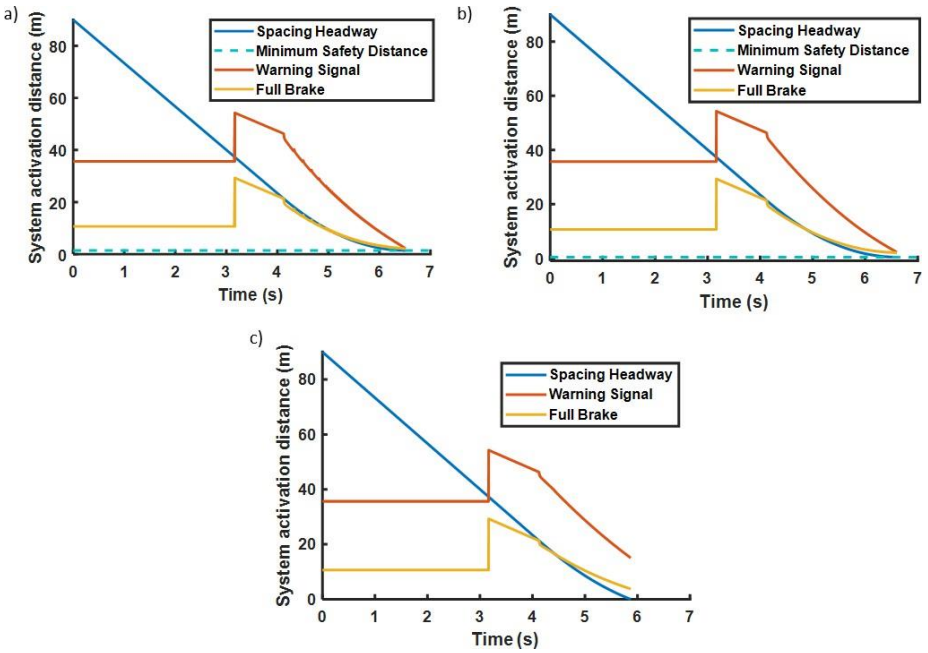

Figure 11. System activation distance against time at (a) μ_{disc} = 0.4, (b) μ_{disc} = 0.35, and (c) μ_{disc} = 0.24 on a wet road surface

3.3 Velocity of the Vehicle and Wheel

Figures 12 (a), (b), and (c) provide graphs of the vehicle's velocity and tire against time. From the results, both vehicle and tire velocity began to decrease at 4.1248 s. Figures 12 (a) and (b) depict the smooth pattern of the decrease of the vehicle velocity and the velocity of each tire. As the brake applied at 4.12 s, the vehicle's and each tire's speed began to slow. However, the result for the brake disc pad friction coefficient = 0.24 in Figure 12 (c) reveals that the car and tire did not stop, and the car crashed against the pedestrian due to the poor coefficient of friction of the brake pad and wet road pavement. Increasing the coefficient of friction of the brake pad could enhance the value of power braking. Conversely, even when the AEB-P is active, a low braking pad friction coefficient reduces the vehicle's safety.

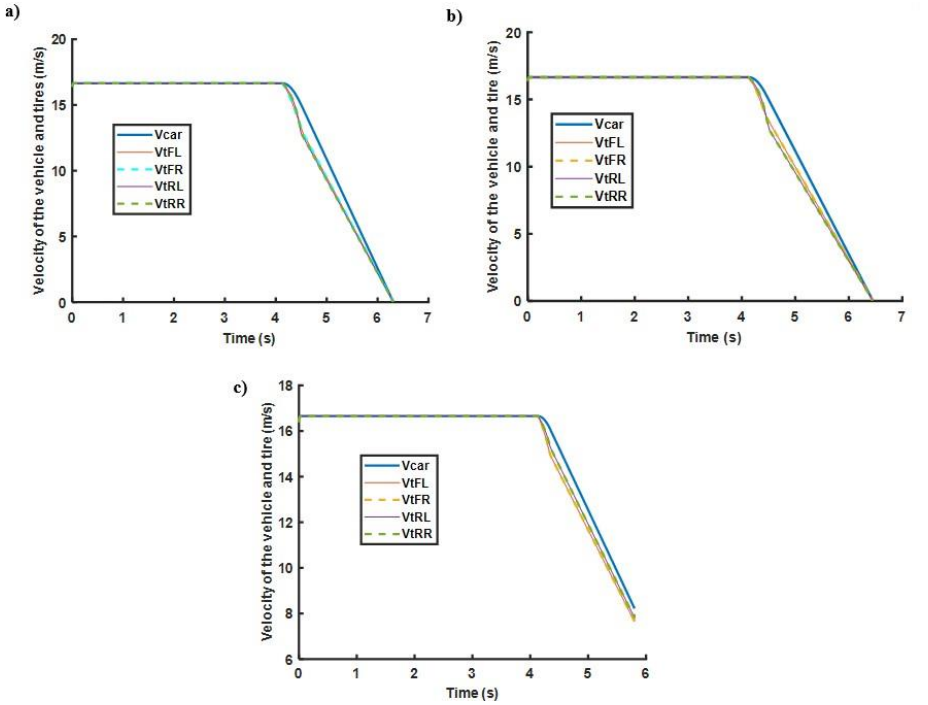

Figure 12. Vehicle's velocity and each tire against time at (a) μ_{disc}= 0.4, (b) μ_{disc}= 0.35, and (c) μ_{disc}= 0.24 on a wet road surface

4.0 CONCLUSION

In this research, a kinematic motion planner simulation framework was used together with VC-APF to maintain the vehicle's minimal safety distance from the pedestrian sliding while braking on wet pavement with varying brake disc pad

friction coefficients. The association of VC-APF and a kinematic path planner is a reliable motion planner for brake emergencies because it provides a warning signal with emergency braking stage distance to the host vehicle. Following emergency braking, the vehicle retained a reasonable minimal safe distance in the 1.5–0.69 m range for brake disc pad friction coefficients of 0.4 and 0.35, respectively. However, when the proposed model simulated a brake pad friction coefficient of 0.24, the vehicle crashed against the pedestrian. These data demonstrate that the suggested design might increase the braking effectiveness and security of the vehicle at a specific brake pad friction coefficient.

5.0 ACKNOWLEDGEMENT

The authors would like to thank the Ministry of Higher Education Malaysia for providing a Fundamental Research Grant Scheme (FRGS/1/2022/TK10/UMP/02/27) (RDU220116). Special thanks to Autonomous Laboratory Universiti Malaysia Pahang Al-Sultan Abdullah for providing the facilities to conduct this study.

6.0 REFERENCES

[1] M. I. Baharuddin, N. K. Khamis, K. A. A. Kassim, and M. R. A. Mansor, "Autonomous Emergency Brake (AEB) for Pedestrian for ASEAN NCAP Safety Rating Consideration: A Review," *Journal of the Society of Automotive Engineers Malaysia*, vol. 3, no. 1, pp. 63-73, 2019.

[2] M. S. Beg and M. Y. Ismail, "Investigation of collision estimation with vehicle and pedestrian using CARLA simulation software," *Journal of Mechanical Engineering and Sciences*, vol. 18, no. 1, pp. 9949–9958, 2024.

[3] H. Wang, Y. Huang, A. Khajepour, Y. Zhang, Y. Rasekhipour, and D. Cao, "Crash Mitigation in Motion Planning for Autonomous Vehicles," *IEEE Transactions on Intelligent Transportation Systems*, vol. 20, no. 9, pp. 3313–3323, 2019.

[4] A. K. Matteo Rizzi Claes Tingvall, "The injury crash reduction of low-speed Autonomous Emergency Braking (AEB) on passenger cars," *In International Research Council on the Biomechanics of Injury*, pp. 656-665, 2014.

[5] M. G. ml Monika Dávideková, "Nice, Berlin, London if every car had autonomous emergency braking system for forward collisions avoidance," *Procedia Computer Science*, vol. 110, pp. 386-393, 2017.

[6] M. Y. Ismail, M. S. Beg, M. F. Jamlos, W. H. Azmi, N. H. Badrulhisam, and O. I. Awad, "Potential and limitation of Internet of Things (IOT) application in the automotive industry: An overview," *International Journal of Automotive and Mechanical Engineering*, vol. 19, no. 3, pp. 9939–9949, 2022.

[7] W. Yang, H. Zhao, and H. Shu, "Simulation and verification of the control strategies for aeb pedestrian collision avoidance system," *Chongqing Daxue Xuebao/Journal of Chongqing University*, vol. 42, no. 2, pp. 1–10, 2019.

[8] U. Z. A. Hamid *et al.*, "Piecewise Trajectory Replanner for Highway Collision Avoidance Systems with Safe-Distance Based Threat Assessment Strategy and Nonlinear Model Predictive Control," *Journal of Intelligent and Robotic Systems*, vol. 90, no. 3, pp. 363–385, 2018.

[9] M. S. Beg, M. Y. Ismail, and M. S. U. Miah, "Evaluating the Performance of a Visual Support System for Driving Assistance using a Deep Learning Algorithm," *Journal of Advanced Research in Applied Sciences and Engineering Technology*, vol. 34, no. 1, pp. 38–50, 2024.

[10] M. Beg, M. Ismail, M. S. U. Miah, and M. Peeie, "Enhancing Driving Assistance System with YOLO V8-Based Normal Visual Camera Sensor," vol. 31, pp. 226–236, 2023.

[11] M. A. H. Ali and M. Mailah, "Path Planning and Control of Mobile Robot in Road Environments Using Sensor Fusion and Active Force Control," *IEEE Transactions on Vehicular Technology*, vol. 68, no. 3, pp. 2176–2195, 2019.

[12] Z. Abdullah, P. M. Heerwan, M. A. Zakaria, and M. I. Ishak, "Investigation of the Combination of Kinematic Path Planning and Artificial Potential Field Path Planning with PI Controller for Autonomous Emergency Braking Pedestrian (AEB-P) System," in *Enabling Industry 4.0 through Advances in Mechatronics*, Springer Nature Singapore, 2022, pp. 285–297.

[13] U. Orozco-Rosas, O. Montiel, and R. Sepúlveda, "Mobile robot path planning using membrane evolutionary artificial potential field," *Applied Soft Computing*, vol. 77, pp. 236–251, 2019.

[14] J. Tang, J. Sun, C. Lu, and S. Lao, "Optimized artificial potential field algorithm to multi-unmanned aerial vehicle coordinated trajectory planning and collision avoidance in three-dimensional environment," *The Proceedings of the Institution of Mechanical Engineers, Part G: Journal of Aerospace Engineering*, vol. 233, pp. 6032–6043, 2019.

[15] H. Hongyu, Z. Chi, S. Yuhuan, Z. Bin, and G. Fei, "An improved artificial potential field model considering vehicle velocity for autonomous driving," *IFAC-PapersOnLine*, vol. 51, no. 31, pp. 863–867, 2018.

[16] P. Raksincharoensak, T. Hasegawa, and M. Nagai, "Motion Planning and Control of Autonomous Driving Intelligence System Based on Risk Potential Optimization Framework," *International Journal of Automotive Engineering*, vol. 7, no. AVEC14, pp. 53–60, 2016.

[17] A. Zulkifli, M. H. Peeie, M. A. Zakaria, M. I. Ishak, M. A. Shahrom, and B. Kujunni, "Motion Planning and Tracking Trajectory of an Autonomous Emergency Braking Pedestrian (AEB-P) System Based on Different Brake Pad Friction Coefficients on Dry Road Surface," *International Journal of Automotive and Mechanical Engineering*, vol. 19, no. 3, pp. 10002–10013, 2022.

[18] E. Šabanovič, V. Žuraulis, O. Prentkovskis, and V. Skrickij, "Identification of Road-Surface Type Using Deep Neural Networks for Friction Coefficient Estimation," *Sensors*, vol. 20, no. 3, 2020.

[19] I. M. Zulhilmi, M. H. Peeie, R. I. M. Eiman, I. M. Izhar, and S. M. Asyraf, "Investigation on vehicle dynamic behaviour during emergency braking at different speed," *International Journal of Automotive and Mechanical Engineering*, vol. 16, no. 1, pp. 6161–6172, 2019.

[20] P. D. Neis, N. F. Ferreira, G. Fekete, L. T. Matozo, and D. Masotti, "Towards a better understanding of the structures existing on the surface of brake pads," *Tribology International*, vol. 105, pp. 135–147, 2017.

[21] O. Towoju, "Braking Pattern Impact on Brake Fade in an Automobile Brake System," *Journal of Engineering Sciences*, vol. 6, pp. E11–E16, Apr. 2019.

[22] M. Kchaou, A. Sellami, R. Elleuch, and H. Singh, "Friction characteristics of a brake friction material under different braking conditions," *Materials & Design (1980-2015)*, vol. 52, pp. 533–540, 2013.

[23] R. Rajamani, "Vehicle Dynamics and Control (2012).pdf," *Mechanical Engineering Series*, Springer New York, 2012.

[24] I. M. Zulhilmi, M. H. Peeie, S. M. Asyraf, I. M. Sollehudin, and I. M. Ishak, "Experimental Study on the Effect of Emergency Braking without Anti-Lock Braking System to Vehicle Dynamics Behaviour," *International Journal of Automotive and Mechanical Engineering*, vol. 17, no. 2, pp. 7832–7841, 2020.

[25] H.-K. Lee, S.-G. Shin, and D.-S. Kwon, "Design of emergency braking algorithm for pedestrian protection based on multi-sensor fusion," *International Journal of Automotive Technology*, vol. 18, no. 6, pp. 1067–1076, 2017.

[26] Y. Saito and P. Raksincharoensak, "Shared Control in Risk Predictive Braking Maneuver for Preventing Collisions With Pedestrians," *IEEE Transactions on Intelligent Vehicles*, vol. 1, no. 4, pp. 314–324, 2016.

[27] W. Yang, X. Zhang, Q. Lei, and X. Cheng, "Research on longitudinal active collision avoidance of autonomous emergency braking pedestrian system (AEB-P)," *Sensors (Switzerland)*, vol. 19, no. 21, 2019.

[28] M. Z. C. Mustafar and S. A. A. Bakar, "Optimal design of an Autonomous Emergency Braking (AEB) system for a passenger vehicle," in *IOP Conference Series: Materials Science and Engineering*, IOP Publishing, 2020, p. 12088.